Indirect dark matter signatures in the cosmic dark ages. I. Generalizing the bound on *s*-wave dark matter annihilation from Planck results

Tracy R. Slatyer[*]

Center for Theoretical Physics, Massachusetts Institute of Technology,
Cambridge, Massachusetts 02139, USA
(Received 18 August 2015; published 25 January 2016)

Recent measurements of the cosmic microwave background (CMB) anisotropies by Planck provide a sensitive probe of dark matter annihilation during the cosmic dark ages, and specifically constrain the annihilation parameter $f_{\text{eff}} \langle \sigma v \rangle / m_\chi$. Using new results (paper II) for the ionization produced by particles injected at arbitrary energies, we calculate and provide f_{eff} values for photons and $e^+ e^-$ pairs injected at keV-TeV energies; the f_{eff} value for any dark matter model can be obtained straightforwardly by weighting these results by the spectrum of annihilation products. This result allows the sensitive and robust constraints on dark matter annihilation presented by the Planck collaboration to be applied to arbitrary dark matter models with *s*-wave annihilation. We demonstrate the validity of this approach using principal component analysis. As an example, we integrate over the spectrum of annihilation products for a range of Standard Model final states to determine the CMB bounds on these models as a function of dark matter mass, and demonstrate that the new limits generically exclude models proposed to explain the observed high-energy rise in the cosmic ray positron fraction. We make our results publicly available at http://nebel.rc.fas.harvard .edu/epsilon.

I. INTRODUCTION

Dark matter (DM) annihilation or other new physics could inject electromagnetically interacting particles into the Universe during its early history, with potentially wide-ranging observable consequences. In particular, injection of ionizing particles during the cosmic dark ages will increase the residual ionization fraction, broadening the last scattering surface and modifying the anisotropies of the cosmic microwave background (CMB) [1–3]. Exquisitely sensitive measurements of the CMB by a range of experiments (e.g. WMAP [4], SPT [5,6] and ACT [7]), and most recently by the Planck satellite [8], can thus place robust and model-independent constraints on such energy injections (e.g. [9–22]).

For the specific case of DM annihilation, precise constraints can be placed under the assumption that the power *deposited* to the gas is directly proportional to that *injected* at the same redshift, with some efficiency factor f_{eff}. More generally, a model- and redshift-dependent effective efficiency factor $f(z)$ can be defined as the ratio of deposited power to injected power at a given redshift (within some arbitrary volume element), even if much of the deposited power originates from energy injections at earlier times. It has been demonstrated [18] that given a set of $f(z)$ functions characteristic of weakly interacting massive particle (WIMP) models for DM [13], the impact on the CMB is identical at the subpercent level, up to an overall

normalization factor, suggesting that approximating $f(z)$ by a constant f_{eff} is reasonable.

In order to convert from deposited power into modifications to the ionization history, the Planck collaboration [8] assumed a simple prescription for the fraction of deposited power proceeding to ionization. This prescription was set by the corresponding fraction for 3 keV electrons, as determined by detailed Monte Carlo studies of the interactions of such electrons by the gas [20,23–26]; we refer to this as the "3 keV" prescription. Earlier papers often took an even simpler approach, the so-called "SSCK" prescription (based on work by Shull and van Steenberg [27], and Chen and Kamionkowski [2]), in which a fraction $(1 - x_e)/3$ of deposited power proceeds into ionization; here x_e is the ionization fraction (as relevant to the gas species in question; if helium is neglected, this is just the hydrogen ionization fraction). In practice, these prescriptions do break down; however, since the ionizing energy produced by a given energy injection is set by the *product* of the deposition-efficiency curve $f(z)$ and the fraction of deposited power proceeding to ionization, any errors in the prescription for the latter may be absorbed as corrections to $f(z)$. The Planck collaboration took this approach, employing corrected $f(z)$ curves, to set limits for several specific DM models: in this paper we employ the same constraints, but demonstrate how to generalize them to a much broader class of DM models (all those where the velocity-weighted annihilation cross section $\langle \sigma v \rangle$ can be treated as constant during the cosmic dark ages).

In an accompanying article [28], referred to as paper II, we have derived new results for the mapping from energy

_____
[*]tslatyer@mit.edu

injection into power contributing to ionization, for e^+e^- pairs and photons injected at arbitrary energy (in the keV to multi-TeV range) and arbitrary redshift (during the cosmic dark ages). Once an energy injection history is specified, the power proceeding into ionization at any redshift can be determined. In particular, in paper II we have provided corrected $f(z)$ curves for DM annihilation (to photons and e^+e^- pairs) that compensate for the inaccuracies in the two most popular ionization prescriptions in the literature, SSCK and 3 keV. The only assumption on the annihilation model, in deriving these curves, is that the redshift dependence of the injected energy is $dE/dVdt \propto (1 + z)^6$ (i.e. the power injected per unit volume is proportional to the square of the density), and that the spectrum of annihilation products is the same at all redshifts. To obtain the $f(z)$ curve for any given model, one need then only integrate over the spectrum of photons and e^+e^- pairs produced by the annihilation.

In this paper we demonstrate that, in accordance with previous studies exploring a smaller range of DM models [16,18,22], the impact of any conventional DM annihilation model on the CMB can be captured by a single normalization factor. The shape of the perturbation to the anisotropy spectrum is independent of the spectrum of annihilation products, and can be accurately obtained by assuming a constant redshift-independent $f(z)$. We derive and present the model-independent weighting function that determines the normalization factor, given a (corrected) deposition-efficiency curve $f(z)$. Having obtained this weighting function, we can convert the corrected $f(z)$ curves presented in paper II directly into $f_{eff}(E)$, for photons and e^+e^- pairs injected by DM annihilation at some arbitrary energy E. Computing f_{eff} for any conventional model of annihilating DM (i.e. one without a novel redshift dependence) is then simply a matter of integrating over the spectrum of annihilation products. As an example, we perform this calculation for the DM masses and Standard Model final states contained in `PPPC4DMID` [29], and determine the resulting constraints from Planck on the annihilation cross sections for these models.

We first review, in Sec. II, the interpretation of the corrected $f(z)$ curves that we employ. In Sec. III we perform a principal component analysis (PCA) to derive the weighting function, construct f_{eff} as a function of injection energy and species, and demonstrate that the f_{eff} results are insensitive to various choices in the analysis. We demonstrate the application of these results to a range of DM models in Sec. IV, and then present our conclusions in Sec. V. The Appendices provide information on supplemental data files, which we make available [30], and review some aspects of PCA and the derivation of the weighting function.

II. THE CORRECTED $f(z)$ CURVES

We use the $f(z)$ curves from paper II [28], and refer the reader to that paper for a detailed description of their derivation. However, it is worth recapping the definition and properties of the three types of $f(z)$ curves we employ, which we will denote $f^{SSCK}(z)$, $f^{3\,keV}(z)$ and $f^{sim}(z)$. In the notation of paper II, these curves correspond to (respectively) $f^{ion,SSCK}(z)$, $f^{ion,3\,keV}(z)$ and $f^{sim}(z)$. We will refer to these curves generally as $f(z)$ curves.

The "ion" superscript indicates that the deposition-efficiency curves have been corrected to ensure that when used with the stated prescription (SSCK or 3 keV), one recovers the correct total power into ionization. This is the appropriate condition for constraints arising from perturbations to the ionization history, which in turn modify the anisotropies of the CMB. It has been shown that in the case of annihilating DM, other deposition channels can essentially be ignored: for example, the limits from high-energy free-streaming photons (discussed briefly in e.g. [3]), distortions to the CMB spectrum [31–34] and modifications to the gas temperature (e.g. [11,21]) are all much weaker (for s-wave-annihilating DM), and ignoring production of Lyman-α photons altogether only changes the constraints by $\sim 5\%$ [16,20]. Accordingly, in this paper we will only ever use $f(z)$ curves corrected to obtain an accurate description of the power proceeding into ionization (in preference to the other deposition channels), and the "ion" superscript is unnecessary.

The $f^{sim}(z)$ curve is obtained from a simplified estimate for the power deposited into each channel. The overall deposited power is corrected by subtracting previously unaccounted power lost into photons below 10.2 eV, which are no longer sufficiently energetic to interact efficiently with the gas (see paper II [28] for details), and then the remainder is multiplied by the SSCK or 3 keV prescription to obtain the power into ionization. This approach is denoted "approx" in [20], in contrast to the "best" treatment that yields the deposition fractions which the $f^{SSCK}(z)$ and $f^{3\,keV}(z)$ functions are designed to reproduce; it relies on the assumption that the SSCK or 3 keV prescriptions are accurate once the energy losses of higher-energy electrons (above 3 keV) to very low-energy photons are taken into account. However, as shown for a range of specific models in [20], this simplified approach gives results comparable to the more detailed calculation.

To summarize, the $f^{SSCK}(z)$, $f^{3\,keV}(z)$ are our best estimates for the appropriate corrected $f(z)$ curves to use with studies that assumed the SSCK or 3 keV prescriptions, respectively; the $f(z)$ curves have been corrected to take into account errors in those prescriptions. The $f^{sim}(z)$ curve is the result of a simpler calculation and can be used as a cross-check. We plot all three sets of curves in Fig. 1, as taken from paper II [28]. Note that all these curves only account for the energy injected by annihilation of the smooth component of DM with the cosmological average density; they do not take into account structure formation at low redshifts. However, it has been shown that the contribution from structure formation to the CMB constraints is generally very subdominant for s-wave annihilation [21].
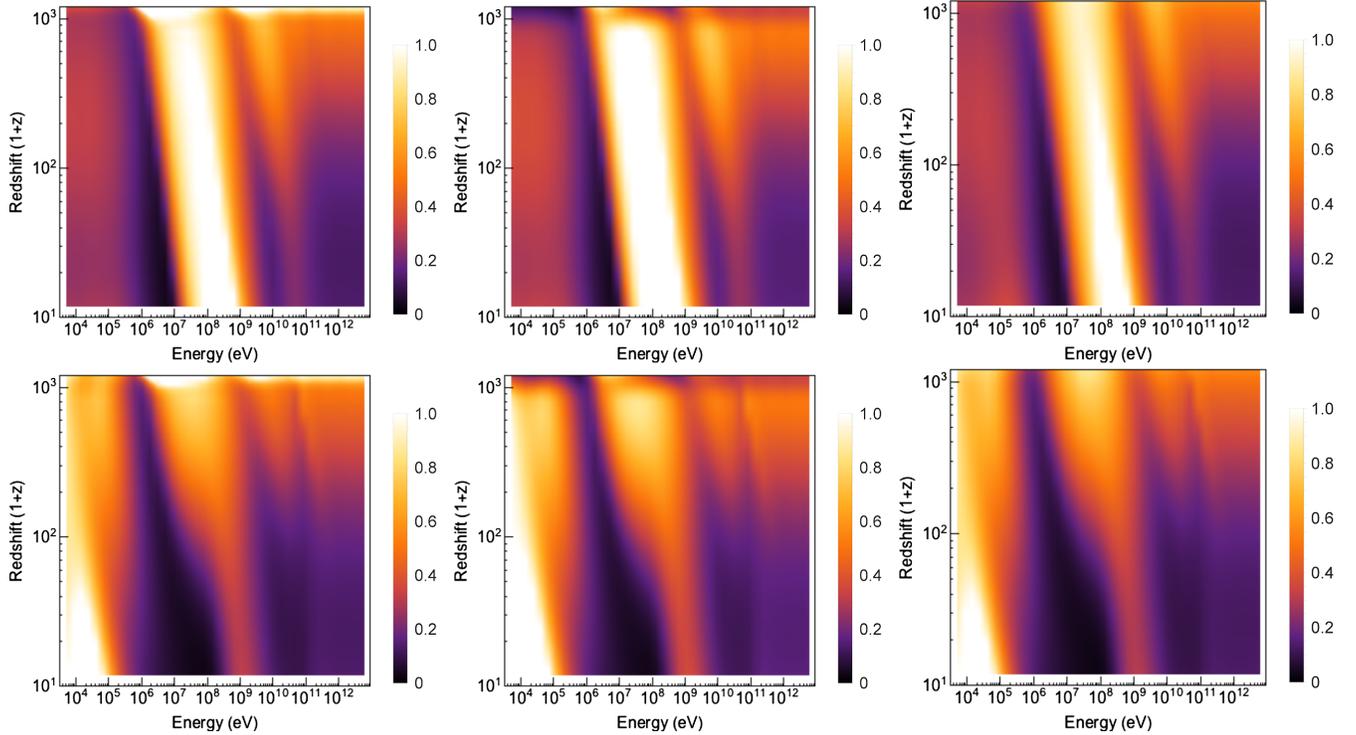
FIG. 1.   Corrected $f(z)$ functions for particles injected by DM annihilation, as a function of injection energy and redshift of absorption. In the left panel we use the 3 keV baseline ionization fractions [so these $f^{3\,\text{keV}}(z)$ curves should be used with analyses that employed the same prescription]; in the center panel we use the SSCK baseline. In the right panel we plot the simplified channel-independent $f^{\text{sim}}(z)$ curve. The upper row describes e^+e^- pairs (the x-axis "energy" label here indicates the kinetic energy of a single member of the pair at injection), the lower row describes photons.

III. CONVERTING CORRECTED $f(z)$ CURVES TO CMB BOUNDS

The most recent and strongest constraints on DM annihilation from CMB anisotropies come from an analysis of Planck data [8]. These constraints were computed using the 3 keV baseline prescription, and were expressed in terms of a bound on $f_{\text{eff}}\langle\sigma v\rangle/m_{\text{DM}}$. For the models tested by those authors, f_{eff} was determined by evaluating the appropriate corrected $f(z)$ curve for the model at $z = 600$, as originally suggested and validated in [17]. Analogous f_{eff} values for arbitrary photon and e^+e^- energies can be read off directly from Fig. 1, using the 3 keV baseline prescription or the simplified $f^{\text{sim}}(z)$ curves (as discussed above, the latter approach is simplified and likely to be less accurate, but it gives a rough estimate of the possible systematic errors arising from details of the first method).

A more careful derivation of f_{eff}—that is, the *constant* value of $f(z)$ which would have the same impact on the CMB as the true corrected $f(z)$ curve—can be achieved by PCA, following the approach of [18].[1] We review the

essentials of the Fisher matrix and PCA in Appendix B. Performing PCA on a range of $f(z)$ curves corresponding to assorted DM models, the authors of [18,22] found that the vast majority of the variance—exceeding 99.9%—was contained in the first principal component, peaking around $z \sim 600$. Related studies [16,17,35] independently determined, using different methods, that the signal was largely controlled by a single parameter, set by the behavior of $f(z)$ at $z \sim 600$.

As described in [22], the "dot product" of a given $f(z)$ curve with the first principal component thus completely determines its detectability. This dot product can be reexpressed as an integral over $d\ln(1+z)$, with the integrand being the product of the $f(z)$ curve with a weighting function $W(z)$. The weighting function can be determined from the first principal component, as described in [18,22]; we provide a detailed derivation in Appendix C. (An alternate PCA, based on the ionization history rather than the energy deposition history, was performed in [36].)

In principle, the weighting function $W(z)$ depends on the details of the experiment (specifically, its sensitivity to different multipoles ℓ, in both temperature and polarization). It will also depend on the ionization prescription, as this affects the mapping between $f(z)$ and the CMB. In practice, however, the impact of these choices turns out to be very small.

---

[1]For convenience, in this paper we use the marginalized Fisher matrices derived and made publicly available by [18]; while those results employed WMAP measurements of the cosmological parameters to determine the fiducial cosmological model, we expect the impact of updating to Planck cosmological parameters to be extremely small.

We performed a new PCA, building our model space from the $f(z)$ curves for annihilation to e^+e^- and photons, for 20 log-spaced energies between 1 keV and 10 TeV (for 40 models total). This is considerably more general than previous studies which focused on the GeV-TeV WIMP parameter space, but again we find that the first principal component overwhelmingly dominates the variance (accounting for more than 99.7% in all cases). In other words, the space spanned by the possible imprints of conventional s-wave DM annihilation on the CMB is (within the confines of the approximate Fisher-matrix approach) essentially one dimensional.

In order to justify computing the constraints on constant $f(z)$ and applying them to arbitrary annihilation models, we need to show that scenarios with constant $f(z)$ also produce a perturbation to the CMB anisotropies lying within this one-dimensional space. To test this question, we consider two energy injection histories, one with $f(z) = \text{constant}$, the other with $f(z)$ given by the first principal component, with the same DM mass and annihilation cross section. Suppose the $f(z)$ curves are normalized such that they correspond to the same signal significance. As discussed in Appendix B (and using the notation defined there), if $\vec{v}_1$ and $\vec{v}_2$ are the discretized version of the $f(z)$ curves, this condition implies $\vec{v}_1^T F_z \vec{v}_1 = \vec{v}_2^T F_z \vec{v}_2$, where F_z is the Fisher matrix (as determined in [18]).

The significance of the difference between these energy injection histories, normalized to the overall significance of either history, can be estimated within the Fisher matrix approach as

$$\sigma_\Delta = \sqrt{\frac{(\vec{v}_2 - \vec{v}_1)^T F_z (\vec{v}_2 - \vec{v}_1)}{\vec{v}_1^T F_z \vec{v}_1}} = \sqrt{2\left(1 - \frac{\vec{v}_2^T F_z \vec{v}_1}{\vec{v}_1^T F_z \vec{v}_1}\right)}. \quad (1)$$

Here we have used the normalization condition above, and also the symmetry of the Fisher matrix to write $\vec{v}_1^T F_z \vec{v}_2 = \vec{v}_2^T F_z \vec{v}_1$. We computed the bracketed quantity on the right-hand side of Eq. (1), taking $f_1(z)$ to be constant and $f_2(z)$ to be the first principal component. We found that in all cases the bracketed quantity was below 0.001, indicating that to a good approximation, the first principal component also captures the effect of constant $f(z)$. Thus it is reasonable to derive constraints on the case of constant $f(z)$ and convert them to constraints on general DM annihilation histories using the weighting function.

We repeated the analysis for each independent combination of the following choices:

(i) A Planck-like experiment vs a cosmic variance limited (CVL) experiment (as defined in [18]).
(ii) Including multipoles up to $\ell = 2500$, vs $\ell = 6000$.
(iii) Using $f^{\text{SSCK}}(z)$, $f^{3\,\text{keV}}(z)$ and $f^{\text{sim}}(z)$ to generate the space of $f(z)$ curves.

(iv) Choosing SSCK vs 3 keV as our baseline ionization prescription [to translate the $f(z)$ curve into its impact on the CMB] when using the $f^{\text{sim}}(z)$ curve.

In all cases we used a Fisher analysis to estimate detectability in the CMB, as described in [18]. We normalized the weighting function as described in [22] and derived in detail in Appendix C, so that $\int W(z) d\ln(1+z) = 1$. Thus for any arbitrary $f(z)$, $\int f(z) W(z) d\ln(1+z)$ measures detectability relative to the case of $f(z) = 1$.

There are visible differences in the weighting functions thus derived, with the largest impacts coming from changing the sensitivity to different multipoles—that is, by considering a Planck-like experiment, vs a CVL experiment up to $\ell = 2500$, vs a CVL experiment up to $\ell = 6000$. However, the resulting variation in f_{eff} computed by the different $W(z)$ functions is always negligible (percent level or less). We show the various $W(z)$ curves in Fig. 2; in Fig. 3 we display the impact on the f_{eff} fractions of scanning over all derived $W(z)$ curves.

We recall that if the $f^{\text{SSCK}}(z)$ and $f^{3\,\text{keV}}(z)$ curves are each used with their specified ionization prescription, they correspond to identical changes to the ionization history. Consequently, their impacts on the CMB must be the same (if contributions from nonionization channels are ignored). However, since the $f(z)$ curves are different, one might expect that the weighting function $W(z)$ will be different—and so must be chosen to match the ionization prescription under which it was derived—in order to compensate. We discuss this point in detail in Appendix D, but it turns out that in practice, the similarity of the different ionization prescriptions and the unit normalization of $W(z)$ means the effect is tiny. Instead, the difference in baseline ionization prescriptions is captured in the f_{eff} parameter, and the derived constraints on that parameter; for example, a higher baseline prescription for ionization would correspond to lower $f(z)$ for all models, and hence lower f_{eff}, but the constraints on a given f_{eff} would be stronger (since the higher ionization prescription corresponds to a larger effect on the CMB).

We have explicitly tested the effect of using the "wrong" weighting function—i.e. using $W(z)$ derived using the $f^{3\,\text{keV}}(z)$ curves, in order to estimate f_{eff} for $f^{\text{SSCK}}(z)$ curves. The effect is included in the bands in Fig. 3, and is negligible.

Consequently, for the purposes of computing f_{eff}, it is entirely adequate to use a single weighting function; we choose the weighting function derived for a CVL experiment including ℓ up to 2500, built from the $f^{3\,\text{keV}}(z)$ curves. We note that this choice is largely arbitrary, as the resulting value of f_{eff} is very stable. This weighting function is likely to be broadly applicable beyond the case of DM annihilation, although it may not capture all the variance for energy injection histories that differ markedly from that of conventional DM annihilation. We leave a
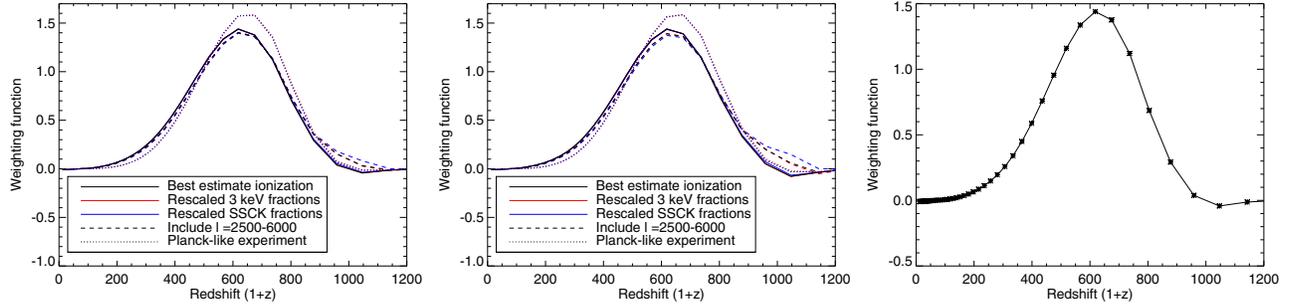
FIG. 2.   Weighting functions for the $f(z)$ curves, derived by PCA. Solid lines show the results for a CVL experiment covering $\ell = 2$–2500, dashed lines show the results for a CVL experiment covering $\ell = 2$–6000, dotted lines show the result for a Planck-like experiment covering $\ell = 2$–2500. *Black* lines use the first procedure for estimating ionization history, *red* lines use the second procedure with 3 keV baseline prescription, *blue* lines use the second procedure with SSCK baseline prescription. Left panel: suitable for 3 keV baseline. Center panel: suitable for SSCK baseline. Right panel: "universal" weighting function recommended for general use.
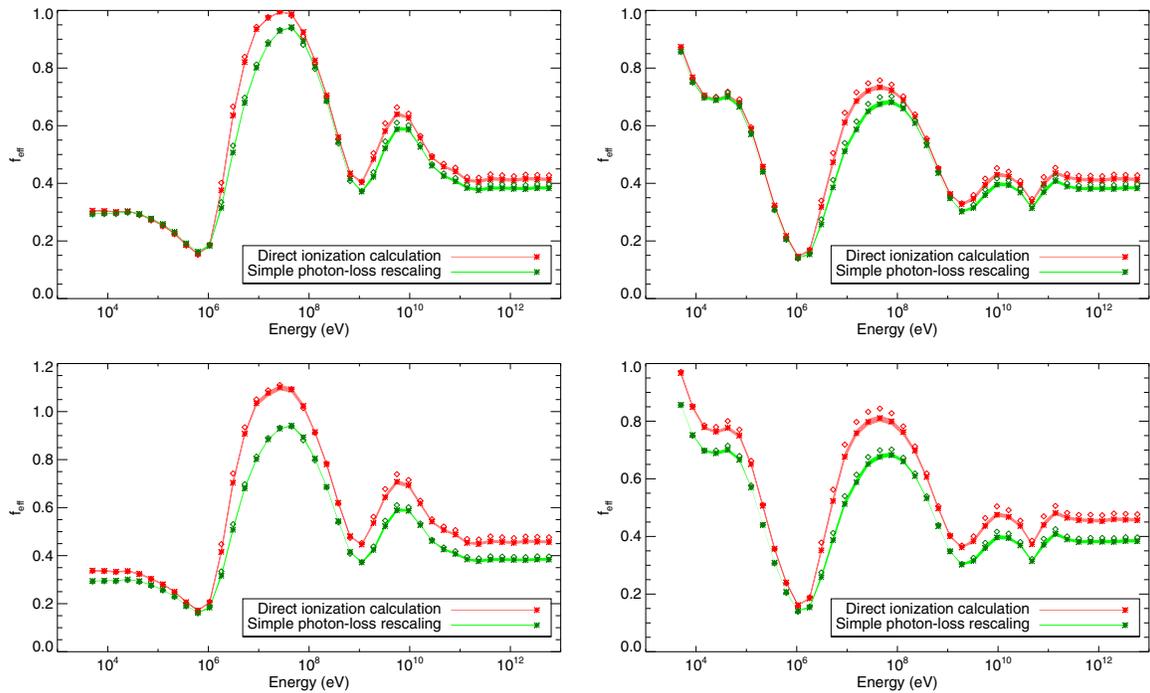

FIG. 3. $f_{\rm eff}$ coefficients as a function of energy for e^+e^- (left column) and photons (right column); appropriate for analyses with baseline prescription 3 keV (top row) or SSCK (bottom row). The widths of the red and green bands indicate the impact of scanning over all the derived weighting functions (see Fig. 2). Red stars are derived from the $f^{\rm SSCK}(z)$ or $f^{3\;\rm keV}(z)$ curves as appropriate (labeled "direct ionization calculation" in the legend), green stars from the $f^{\rm sim}(z)$ curves (labeled "simple photon-loss rescaling" in the legend). Diamonds indicate $f_{\rm eff}$ evaluated as $f(600)$, rather than using a weighting function.

more detailed PCA, based on a larger range of possible injection histories, for future work.

One can integrate any electron and photon spectra produced by DM annihilation over the $f_{\rm eff}$ curves presented in Fig. 3, in order to determine $f_{\rm eff}$ for an arbitrary model. We show results separately for the 3 keV and SSCK baseline prescriptions; however, when making comparisons with the Planck constraints [8], the 3 keV baseline prescription should always be used. We also show the

effect of taking our second simplified procedure for computing $f_{\rm corr}(z)$, and the effect of evaluating $f_{\rm corr}(600)$ rather than using the weighting function; both effects are rather small, at the $< 10\%$ level.

The $f_{\rm eff}$ curves (Fig. 3) exhibit significant structure as a function of energy. At high energies, both e^+e^- pairs and photons asymptote to $f_{\rm eff} \approx 0.4$; this convergent behavior is expected, since at high energies electrons and photons both participate in a pair production/inverse Compton scattering

(ICS) cascade. Both species demonstrate some minor structure in the GeV-TeV range but generally maintain $f_{\rm eff} \sim 0.4$, with a peak of $f_{\rm eff} \sim 0.7$ for electrons at injection energies around 10 GeV. Both species then exhibit a large bump in $f_{\rm eff}$, peaking at energies around 10–100 MeV, and a trough at $\mathcal{O}(\rm MeV)$ energies. This trough occurs because mildly relativistic electrons suffer large losses into continuum photons with energies below 10.2 eV (see paper II [28] for an in-depth discussion). Accordingly, MeV-scale electrons have small $f_{\rm eff}$, and the dominant energy loss process for MeV-scale photons is Compton scattering, which in turn produces more mildly relativistic electrons. The peak at slightly higher energy occurs because 10–100 MeV electrons lose most of their energy by inverse Compton scattering into $\mathcal{O}(100{-}10^4)$ eV photons, which are efficient ionizers.

At low energies, below $\sim$1–100 keV (depending on the redshift), photons become efficient photoionizers, causing a large $f_{\rm eff}$. In contrast, the e^+e^- $f_{\rm eff}$ at low kinetic energies is rather low, of order 0.3—but as noted in [19], this is because in the context of DM annihilation, almost all the injected power is bound up in the mass energy of the pair in this case. Consequently, the absorption of the kinetic energy is almost irrelevant: what matters is the absorption of the photons produced when the positron annihilates. From inspection of $f_{\rm eff}$ for $\sim$0.5 MeV photons, one would expect $f_{\rm eff}$ of 0.3 for pairs produced nearly at rest, consistent with the results of the calculation.

The primary systematic uncertainties in this calculation arise from the choice of $f(z)$ curves [$f^{\rm SSCK,3\ keV}(z)$ or $f^{\rm sim}(z)$]. Both of these curves involve an approximation; on one hand matching the power into ionization exactly (up to the limitations of our approximate treatment of the low-energy photons) while not attempting to match the heating and Lyman-α channels, on the other approximating *all* channels by the cooling of 3 keV electrons after accounting for energy lost to continuum photons. Some approximation of this form is inevitable, given that the true relative losses into the different channels are *not* independent of the injected particle energy as tacitly assumed by both the SSCK and 3 keV prescriptions. As discussed more extensively in [20], we estimate the potential systematic error due to these approximations and our simplified treatment of the low-energy photons to be at the $\sim$10% level. For some channels, the constraints we present may also be slightly too conservative, i.e. weaker than the true limits, at a similar $\sim$10% level, due to our neglect of energy deposition by protons and antiprotons [37].

IV. CONSTRAINTS FOR SIMPLE ANNIHILATION CHANNELS

In this section we apply the results of this paper to the Standard Model final states provided in the PPPC4DMID package [29], following the earlier analysis by [38]. PPPC4DMID provides the fluxes of positrons and photons

produced by DM annihilation to 28 Standard Model final states, for masses ranging from 5 GeV to 100 TeV. The fluxes include electroweak final state radiation [39], which can be crucial at high DM masses; thus, for example, there is a small but nonzero $f_{\rm eff}$ for annihilation to $\nu\bar{\nu}$, arising from the electroweak corrections.

We only show results up to 10 TeV, as above this mass, additional processes not considered in [13] may contribute to the cooling of electrons and photons in the early Universe. However, we expect that the $f_{\rm eff}$ results will be similar at higher DM masses, since the processes neglected in [13] will only modify the details of the pair production cascade experienced by particles injected at high energy, which occurs much faster than a Hubble time and so is anticipated to have little effect on the fraction of power eventually deposited.

We take the positron and photon spectra provided in PPPC4DMID [40], assume that by charge symmetry the spectrum of e^- is equal to that of e^+, and integrate the resulting e^+e^- and photon spectra over the $f_{\rm eff}(E)$ curves presented in Fig. 3. Specifically, if a given annihilation produces a spectrum $(dN/dE)_{e^+}$ of positrons, and a spectrum $(dN/dE)_\gamma$ of photons, the weighted $f_{\rm eff}(m_\chi)$ curve is given by

$$f_{\rm eff}(m_\chi) = \frac{\int_0^{m_\chi} E\, dE[2 f_{\rm eff}^{e^+e^-}(E)(\frac{dN}{dE})_{e^+} + f_{\rm eff}^\gamma(E)(\frac{dN}{dE})_\gamma]}{2m_\chi},$$

(2)

where E is the energy of the positron or photon (the factor of 2 comes from the electron spectrum).

We use the best-estimate $f_{\rm eff}(E)$ curves suited for the 3 keV baseline prescription, as we wish to apply the constraints derived by the Planck collaboration [8]. We take the Planck limit to be $f_{\rm eff}\langle\sigma v\rangle/m_\chi < 4.1 \times 10^{-28}$ cm^3/s/GeV, which is the bound set by the Planck temperature and polarization data. The limit can be strengthened by $\sim$15% by the inclusion of either lensing or external data sets. We show both the $f_{\rm eff}(m_\chi)$ curves for each channel and the resulting constraints on the annihilation cross section in Fig. 4. For DM masses below 5 GeV, we show estimated limits for DM annihilation to e^+e^-, $\gamma\gamma$ or $VV \to 4e$—the last channel corresponds to DM annihilating to a pair of intermediate vector bosons, each of which subsequently decays to e^+e^-. The results for the first two channels are taken simply from Fig. 3, whereas for $VV \to 4e$, the e^+e^- spectrum is taken to be constant in dN/dE between the kinematic limits $m_e < E < m_\chi - m_e$. For both channels producing e^+e^-, there will also be an FSR contribution, but its effect is generally small (at the percent level).

In general, we see that the final states considered fall into three categories:

(i) Final states where the bulk of the power proceeds into e^+e^- and photons, where at masses

FIG. 4.   The upper panel shows the $f_{\rm eff}$ coefficients as a function of DM mass for each of a range of SM final states, as indicated in the legend. The $VV \to 4X$ states correspond to DM annihilating to a pair of new neutral vector bosons V, which each subsequently decay into e^+e^-, $\mu^+\mu^-$ or $\tau^+\tau^-$ (labeled by X). The lower panels show the resulting estimated constraints from recent Planck results [8], as a function of DM mass, for each of the channels. The left panel covers the range from keV-scale masses up to 5 GeV, and only contains results for the e^+e^-, $\gamma\gamma$ and $VV \to 4e$ channels; the right panel covers the range from 5 GeV up to 10 TeV, and covers all channels provided in the PPPC4DMID package [29]. The light and dark gray regions in the lower right panel correspond to the 5σ and 3σ regions in which the observed positron fraction can be explained by DM annihilation to $\mu^+\mu^-$, for a cored DM density profile (necessary to evade γ-ray constraints), taken from [41]. The solid yellow line corresponds to the preferred cross section for the best fit 4-lepton final states identified by [42], who argued that models in this category can still explain the positron fraction without conflicts with nonobservation in other channels. The red and black circles correspond to models with $4e$ (red) and 4μ (black) final states, fitted to the positron fraction in [43]; as in that paper, filled and open circles correspond to different cosmic-ray propagation models. The near-horizontal dashed gold line corresponds to the thermal relic annihilation cross section [44].

above 100 GeV the constraint approaches $\langle \sigma v \rangle \lesssim 10^{-27}(m_\chi/1~{\rm GeV})~{\rm cm}^3/{\rm s}$.

(ii) Annihilation to neutrinos, where the constraint arises entirely from electroweak corrections, and is negligible below ~ 200 GeV; at $\mathcal{O}({\rm TeV})$ masses, cross sections as low as a few $\times 10^{-23}~{\rm cm}^3/{\rm s}$ can be constrained. Interestingly, this bound is competitive with that placed by IceCube from observations of galaxy clusters [45], the Galactic Center [46], and the Milky Way halo [47], and unlike those limits is independent of uncertainties in the local DM density, the DM distribution, and the amount of DM substructure.

(iii) A band with a width of roughly a factor of 150% in $\langle \sigma v \rangle$ that encompasses all the other channels studied, which at high masses corresponds to $\langle \sigma v \rangle \lesssim 2 - 3 \times 10^{-27}(m_\chi/1~{\rm GeV})~{\rm cm}^3/{\rm s}$.

Accordingly, for any linear combination of these final states that does not contain a significant branching ratio for DM annihilation directly to neutrinos, one must have $\langle \sigma v \rangle \lesssim 3 \times 10^{-27}(m_\chi/1~{\rm GeV})~{\rm cm}^3/{\rm s}$. It is thus challenging to obtain the correct thermal relic cross section for s-wave annihilating DM with mass much below $m_\chi \sim 10$ GeV, without violating these limits (although models with suppressed annihilation at late times may still be viable, e.g. asymmetric DM models or the scenarios proposed in [48,49]). At higher masses, the cross sections constrained are well above the thermal relic value, but are highly relevant for DM explanations of the positron excess observed by PAMELA [50], Fermi [51] and AMS-02 [52]. For example, the authors of [42] identified a favored scenario by which to explain this excess via DM annihilation, respecting all existing constraints: 0.5–1 TeV DM annihilating through a light mediator to a mixture of 75%

$\tau^+\tau^-$ and 25% e^+e^-. The required cross section is roughly $\langle\sigma v\rangle \sim 5\times 10^{-24}$ cm^3/s at 500 GeV and roughly $\sim 1.5\times 10^{-23}$ cm^3/s at 1 TeV. This is clearly above the bounds for the contributing annihilation channels in Fig. 4. Similarly, the authors of [43] found that only annihilation through a light mediator to muons or electrons could explain the excess without violating bounds from studies of dwarf galaxies in gamma rays. The preferred cross section was ~ 1.3–1.6×10^{-24} cm^3/s at a DM mass of ~ 350 GeV for the $4e$ final state, and ~ 6–8×10^{-24} cm^3/s at a DM mass of ~ 600–750 GeV for the 4μ final state. Again, these preferred points are well above the bounds we derive for the corresponding channels.

Figure 4 shows (1) the cross section band favored for the models of [42] as a solid yellow line, (2) the points favored by [43] as circles in red ($4e$ final state) or black (4μ final state), and (3) a gray contour describing the region in which DM annihilation to $\mu^+\mu^-$ can explain the AMS-02 data [41]. These favored regions should be compared, respectively, to (1) an appropriately weighted combination of the green dot-dashed and red dot-dashed lines in Fig. 4 (it is a conservative choice to take the green dot-dashed line to set the limit), (2) the red dot-dashed and black dot-dashed lines, and (3) the solid black line. We see that in general these models are ruled out by more than a factor of 2, and up to an order of magnitude. The models presented in [53] were studied in [8], and are similarly ruled out by these constraints.

V. CONCLUSIONS

In this paper, we have mapped out the effective deposition efficiency, $f_{\rm eff}$, for photons and e^+e^- pairs injected into the early Universe by DM annihilation, at $\mathcal{O}$(keV-TeV) kinetic energies. We have made our key numerical results publicly available online [30].

We have demonstrated that it is sufficient to use a simple universal weighting function to convert any redshift-dependent energy deposition history (originating from conventional s-wave-dominated DM annihilation) into a redshift-independent efficiency factor, confirming earlier results for the WIMP regime. This efficiency factor then converts Planck limits on energy injection from the CMB into constraints on the DM model in question. Any DM model featuring dominantly s-wave annihilation, with the only redshift dependence in the annihilation rate arising from the DM density squared, can thus be constrained using these data. We emphasize that this does not subsume the limits presented by the Planck collaboration, but confirms the validity of the procedure employed in that analysis, and demonstrates how to extend those bounds to more general DM models.

We have performed an example calculation for 28 different annihilation channels over the DM mass range 5 GeV–10 TeV, and demonstrated that except for annihilation directly into neutrinos, at high masses the constraint

from the CMB generically lies in the range $\langle\sigma v\rangle \lesssim 1$–$3\times 10^{-27}(m_\chi/1\text{ GeV})$ cm^3/s. Even for annihilation to neutrinos, at TeV-scale masses we can set an upper bound on the cross section of order a few times 10^{-23} cm^3/s, comparable to constraints from IceCube observations of the Milky Way and galaxy clusters; this bound arises from electroweak final state radiation producing e^+e^- pairs and photons.

The constraints we obtain appear to rule out annihilating DM models proposed to explain the observed excess of cosmic-ray positrons, including models which could not be excluded by any previous studies. This constraint could be evaded if the DM annihilation is suppressed at low velocities or early times.

APPENDIX A: SUPPLEMENTARY MATERIALS

We make available [30] a selection of `.fits` and `.dat` files containing the $f_{\rm eff}$ values presented in Figs. 3 and 4 (with the exception of the $VV\to 4e$ channel below 5 GeV, which can be trivially obtained—at least at the level we have calculated it—from the results for e^+e^-), as well as the universal annihilation weighting function shown in Fig. 2. We also provide an example Mathematica notebook to demonstrate the use of the `.fits` files.

The `.fits` files are as follows:

`feff_summary_species_base.fits`

Here "species" can be "elec" (representing e^+e^- pairs) or "phot" (representing photons), and "base" can be SSCK or 3 keV, corresponding to the choice of baseline ionization prescription. For example, the 3 keV files should be used with the constraints on DM annihilation of [8]. Each file contains the following arrays:

(i) REDSHIFT: This 63-element array provides the abscissa for deposition redshift.

(ii) WEIGHTFN: This 63-element array provides the weighting function shown in the third panel of Fig. 2, sampled at the redshifts given by the

REDSHIFT array, and normalized so that $\int W(z)\,d\ln(1+z) = 1$ (up to numerical error).

(iii) LOG10ENERGY: This 40-element array gives $\log_{10}(E/\text{eV})$, where E is the kinetic energy of one member of the pair of injected particles (for e^+e^- pairs) or the energy of a single injected photon.

(iv) FEFF_BEST: This 40-element array gives f_{eff} computed using the appropriate $f^{\text{base}}(z)$ curve, weighted by the weighting function.

(v) FEFF_RESCALING: This 40-element array gives f_{eff} computed using the appropriate $f^{\text{sim}}(z)$ curve, weighted by the weighting function.

(vi) FEFF_BEST_600: This 40-element array gives f_{eff} computed using the appropriate $f^{\text{base}}(z)$ curve, evaluated at $z = 600$.

feff_PPPC_3 keV.fits

This file contains the f_{eff} curves for different DM masses and annihilation channels as shown in Fig. 4, at DM masses above 5 GeV. Below 5 GeV, the results for the e^+e^-, $\gamma\gamma$ and $VV \to 4e$ channels are easily obtained from the feff_summary_species_3 keV.fits files. The arrays in this file are

(i) DM_MASS: This 62-element array gives the DM mass in GeV.

(ii) CHANNEL: This 28-element array labels the channels as shown in the legend of Fig. 4.

(iii) FEFF: This 28×62 array contains the f_{eff} values for each DM mass and channel, derived using the appropriate $f^{3\,\text{keV}}(z)$ curves and the weighting function.

The .dat files simply contain condensed summaries of the .fits files, and are as follows:

feff_PPPC_3 keV.dat

As feff_PPPC_3 keV.fits, except that the f_{eff} values are laid out in a grid, with columns corresponding to different channels (the first row describes the different final states) and rows corresponding to different DM masses (the first column gives the DM mass in GeV).

feff_base.dat

This contains a subset of the information in feff_summary_electron_base.fits and feff_summary_photon_base.fits: the first column is the LOG10ENERGY array from these files, describing the injection energy; the second is the best-estimate f_{eff} value [computed using the $f^{\text{base}}(z)$ curves and the weighting function] for e^+e^- pairs; the third is the best-estimate f_{eff} for photons. "base" can take the values SSCK or 3 keV and should be chosen based on the ionization prescription used in the analysis to which comparison is desired.

weighting_function.dat

This contains the weighting function $W(z)$ shown in the third panel of Fig. 2, sampled at the redshifts $1 + z$ given in the first column.

APPENDIX B: REVIEW OF PRINCIPAL COMPONENT ANALYSIS

Suppose we have some arbitrary energy deposition history, characterized by a (corrected) efficiency function $f(z)$. Let us discretize the $f(z)$ function into n_z bins centered at z_i, $i = 1, …, n_z$, thus describing the energy deposition by a column vector $\vec{v} = (f(z_1), f(z_2), f(z_3), …, f(z_{n_z}))$. We follow [18] in treating the energy deposition profile $f(z)$ in each bin as a Gaussian in $\ln(1+z)$, normalized such that its integral with respect to $d\ln(1+z)$ is equal to the logarithmic bin width $\Delta \ln(1+z)$.

Within the approximation of linearity (which is a good approximation for energy injections at the level constrained by Planck [18]), the impact of this deposition history on the anisotropies of the cosmic microwave background can be written in the form

$$h \equiv \Delta C_\ell = T\vec{v}, \tag{B1}$$

where T is some transfer matrix of dimension $n_\ell \times n_z$, and n_ℓ is the number of multipoles we consider. Following [18], in our notation each element of T ($T_{\ell i}$) is itself a three-element vector, holding the perturbations to the TT, TE and EE anisotropy spectra at that ℓ. T can be computed element by element, as described in [18], by taking $\vec{v}_j$ such that $v_i = \delta_{ij}$, and computing the effects on the CMB using RECFAST [54] (or a similar code such as CosmoRec [55] or HyRec [56]) and CAMB [57]. Similarly, we can determine a corresponding $n_\ell \times 6$ transfer matrix describing the effect of varying the standard six cosmological parameters.

Once T has been mapped out, we can construct the $n_z \times n_z$ Fisher matrix F_e as

$$(F_e)_{ij} = \sum_\ell T_{\ell i}^T \cdot \Sigma_\ell^{-1} T_{\ell j}, \tag{B2}$$

where Σ_ℓ is the appropriate covariance matrix for the anisotropy spectra (see [18] for the explicit form). Schematically, $F_e = T^T \Sigma^{-1} T$; it is a symmetric matrix, due to the symmetry of Σ, and its diagonal elements $(F_e)_{ii}$ describe the (squared) signal significance per energy deposition at redshift z_i, before marginalization over the existing cosmological parameters.

To perform this marginalization, one first constructs an expanded Fisher matrix F_0, using Eq. (B2) but expanding T to include the effect of the standard six cosmological parameters. We can write

$$F_0 = \begin{pmatrix} F_e & F_v \\ F_v^T & F_c \end{pmatrix}, \tag{B3}$$

where F_e is the premarginalization Fisher matrix as defined above, F_c is the Fisher matrix for the cosmological parameters only, and F_v describes the cross terms. Then

the *marginalized* Fisher matrix, describing the detectability of an energy injection after projecting out the perturbations parallel to the standard cosmological parameters, is given by $F_z = F_e - F_v F_c^{-1} F_v^T$ (see [18] for a discussion).

The principal components are given by the eigenvectors of F_z, which we will denote $\{\vec{P}_i\}$, $i = 1, ..., n_z$. By construction, they form an orthogonal basis for arbitrary $f(z)$ histories, and we can choose them to be orthonormal; as such, one can write the vector corresponding to any arbitrary $f(z)$ in the form $\vec{v} = \sum \alpha_i \vec{P}_i$, where $\vec{P}_i$ is the *i*th principal component and $\alpha_i = \vec{v} \cdot \vec{P}_i$. Each principal component perturbs the CMB anisotropies with significance proportional to the square root of the corresponding eigenvalue (to the degree that the approximations inherent in the Fisher matrix analysis are valid). Consequently, if the principal components are ranked in order of their eigenvalues, the detectability of an arbitrary energy deposition history can be described approximately by $\alpha_1 = \vec{v} \cdot \vec{P}_1$, the dot product with the first principal component. In this sense, $\vec{P}_1$ acts as a redshift-dependent weighting function that determines the detectability of an arbitrary energy deposition history. The accuracy of this "weighting function" approximation will be controlled by the fraction of the total variance described by the first eigenvalue (it may also break down for specific energy deposition histories where $\vec{v}$ is accidentally nearly orthogonal to $\vec{P}_1$).

APPENDIX C: DERIVING THE UNIVERSAL WEIGHTING FUNCTION FOR ANNIHILATING DM

Rather than working in terms of energy deposition histories localized in redshift, one can perform a similar PCA starting with any sample of $f(z)$ functions (see [18] for a more complete discussion); the resulting principal components will be applicable to any energy deposition history lying within the space spanned by these basis functions. For the purposes of setting CMB constraints, any conventional DM annihilation model can be described as a linear combination of photons and $e^+ e^-$ pairs injected over a range of energies.

Consequently, we can perform a PCA applicable to all conventional DM annihilation models, by taking as our basis functions the $f(z)$ curves plotted in Fig. 1. We choose 20 log-spaced injection energies for photons and $e^+ e^-$ pairs, thus giving rise to 40 $f(z)$ curves as our sample. As previously, we can sample these curves at n_z redshifts, translating them into n_z-element column vectors, which we will denote $\vec{u}_i$ for $i = 1, ..., 40$. (More generally, we will denote the number of models included in the PCA as n_M: in this case $n_M = 40$.) Let U be the $n_z \times n_M$ matrix with the *i*th column given by $\vec{u}_i$. A general DM annihilation model can be expressed as $\vec{v} = U\vec{\alpha}$, where $\vec{\alpha}$ now describes the coefficients of the (*not* orthogonal) basis vectors $\vec{u}_i$. Thus

we can describe the matrix U as mapping from n_M-dimensional "coefficient space" into n_z-dimensional "redshift space."

Following the same procedure as previously, we can compute the impact on the CMB of each of the $\vec{u}_i$ histories, thus constructing a $n_\ell \times n_M$ transfer matrix T_M that maps from coefficient space to the anisotropies of the CMB. In terms of the earlier transfer matrix T, $T_M = TU$. Let us label the associated $n_M \times n_M$ Fisher matrix (after marginalization over the standard cosmological parameters) as F_M, and the expanded premarginalization Fisher matrix as F_{0M}.

Since the transfer matrix for the cosmological parameters is unchanged, writing T_M in terms of T yields the following relation between F_0 and F_{0M}:

$$F_{0M} = \begin{pmatrix} U^T F_e U & U^T F_v \\ (U^T F_v)^T & F_c \end{pmatrix}. \quad (C1)$$

Consequently, the marginalized Fisher matrix becomes

$$F_M = U^T F_e U - U^T F_v F_c^{-1} F_v^T U = U^T F_z U. \quad (C2)$$

Diagonalizing F_M now yields a set of principal components specialized to the case of DM annihilation; these principal components are n_M-element vectors, and describe coefficient vectors $\vec{\alpha}$ for the original basis $f(z)$ curves. Accordingly, they are orthonormal in coefficient space, *not* redshift space. If we denote these principal components as $\{\vec{p}_i\}$, $i = 1, ..., n_M$, then following the reasoning above, we can write $\vec{\alpha} = \sum_i (\vec{\alpha} \cdot \vec{p}_i) \vec{p}_i$, and the detectability of the energy deposition history characterized by the coefficient vector $\vec{\alpha}$ is determined approximately by $\vec{\alpha} \cdot \vec{p}_1$.

Due to the similarity of the $f(z)$ curves for different energies and different species, when the eigenvalues are calculated, the first principal component accounts for more than 99% of the variance. Accordingly, having specialized to the case of DM annihilation, the weighting function approximation is expected to be accurate at the subpercent level.

However, we would prefer to express this dot product directly in terms of the energy deposition history $f(z)$, or its discretized counterpart $\vec{v}$, rather than its coefficients with respect to a somewhat arbitrary basis. To achieve this, note that since $\vec{v} = U\vec{\alpha}$, we can write

$$U^T F_z \vec{v} = U^T F_z U\vec{\alpha} = F_M \sum_{i=1}^{m_N} (\vec{\alpha} \cdot \vec{p}_i) \vec{p}_i = \sum_{i=1}^{m_N} \lambda_i (\vec{\alpha} \cdot \vec{p}_i) \vec{p}_i. \quad (C3)$$

Here λ_i is the *i*th eigenvalue of F_M, and so $F_M \vec{p}_i = \lambda_i \vec{p}_i$ by definition. Taking the dot product with $\vec{p}_1$ then yields

$$p_1 \cdot (U^T F_z \vec{v}) = \lambda_1 (\vec{\alpha} \cdot \vec{p}_1), \quad (C4)$$

and consequently,

$$\vec{\alpha} \cdot \vec{p}_1 = \frac{1}{\lambda_1} p_1^T U^T F_z \vec{v} = \left(\frac{(U\vec{p}_1)^T F_z}{\lambda_1} \right) \cdot \vec{v}. \quad \text{(C5)}$$

If a constraint on *some* deposition history $f_0(z)$ (lying within the space spanned by conventional DM annihilation) has been computed, therefore, the constraint on any *other* $f(z)$ (at the same DM mass and cross section) can be computed by rescaling the bound by a factor:

$$f_{\text{eff}} = \frac{\left(\frac{(U\vec{p}_1)^T F_z}{\lambda_1} \right) \cdot \vec{v}}{\left(\frac{(U\vec{p}_1)^T F_z}{\lambda_1} \right) \cdot \vec{v}_0} = \left[\frac{(U\vec{p}_1)^T F_z}{((U\vec{p}_1)^T F_z) \cdot \vec{v}_0} \right] \cdot \vec{v}. \quad \text{(C6)}$$

A higher f_{eff} corresponds to a more detectable $f(z)$, and hence to a stronger bound. The quantity in square brackets now acts as a weighting vector $\vec{W}$ which converts $\vec{v}$ to f_{eff}. In principle, we could use any vector $\vec{v}_0$ to determine the reference bound, but in practice the usual choice is $f(z) = 1$, so f_{eff} represents "effective deposition efficiency" relative to the case corresponding to total prompt energy deposition (with one of the simplified ionization prescriptions). This choice yields

$$\vec{W} = \frac{(U\vec{p}_1)^T F_z}{\sum_i ((U\vec{p}_1)^T F_z)_i}. \quad \text{(C7)}$$

We can define a *continuous* weighting function $W(z)$ by interpolation, fixing

$$W(z_i) = \frac{(\vec{W})_i}{d \ln(1+z)}. \quad \text{(C8)}$$

Then the normalization condition $\sum_i (\vec{W})_i = 1$ translates into $\sum_i W(z_i) d \ln(1+z) = 1$, and so when the continuous limit is taken, $\int W(z) d \ln(1+z) = 1$. We can likewise rewrite f_{eff} in terms of the continuous functions $f(z)$ and $W(z)$,

$$f_{\text{eff}} = \sum_i f(z_i)(\vec{W})_i = \sum_i f(z_i) W(z_i) d \ln(1+z)$$

$$\rightarrow \int f(z) W(z) d \ln(1+z). \quad \text{(C9)}$$

This is the weighting function provided in the main text.

APPENDIX D: EXPECTED CHANGE TO THE WEIGHTING FUNCTION DUE TO IONIZATION PRESCRIPTION

As discussed in Sec. III, the weighting function has some dependence on the presumed baseline ionization prescription, even though the $f^{\text{SSCK}}(z)$ and $f^{3 \text{ keV}}(z)$ curves

correspond to identical physical ionization histories (when properly combined with the appropriate ionization prescriptions). There is also a *separate* dependence on the presumed baseline ionization prescription when the $f^{\text{sim}}(z)$ curve is used, but in this case the dependence is physical; it affects the mapping from DM models into the CMB, by changing the transfer matrix T_M (and T).

In the notation of Appendix C, when $f^{\text{SSCK}}(z)$ or $f^{3 \text{ keV}}(z)$ curves are used, the F_M Fisher matrix (and resulting principal components) are unaffected by the choice of ionization prescription, as these depend only on the (physical) CMB signatures of particular DM annihilation models. However, the U and F_z matrices, which involve mappings between DM models and $f(z)$ curves, or $f(z)$ curves and the CMB, *are* affected.

Let U_1 and U_2 denote the matrices that hold the $f(z)$ curves for two different baseline ionization prescriptions, and let $i_1(z)$, $i_2(z)$ describe the fraction of deposited power proceeding into ionization (as a function of redshift) in those two prescriptions. Let I_1 and I_2 define the $n_z \times n_z$ diagonal matrices such that $(I_a)_{jk} = i_a(z_j)\delta_{jk}$. Then since by the definition of $f^{\text{base}}(z)$ curves, the power into ionization at any redshift is invariant, we can write $I_1 U_1 = I_2 U_2$.

Now if F_{z1} and F_{z2} are the Fisher matrices corresponding to the two baseline ionization prescriptions, we can write $F_M = U_1^T F_{z1} U_1 = U_1^T I_1 I_1^{-1} F_{z1} I_1^{-1} I_1 U_1 = U_2^T I_2 I_1^{-1} F_{z1} I_1^{-1} I_2 U_2 = U_2^T F_{z2} U_2$. It follows that

$$F_{z2} = I_2 I_1^{-1} F_{z1} I_1^{-1} I_2. \quad \text{(D1)}$$

Then we can immediately write down the relationship between the weighting vectors corresponding to the two prescriptions,

$$\begin{aligned} \vec{W}_2 &= \frac{(U_2\vec{p}_1)^T F_{z2}}{\sum_i ((U_2\vec{p}_1)^T F_{z2})_i} \\ &= \frac{(I_2^{-1} I_1 U_1 \vec{p}_1)^T I_2 I_1^{-1} F_{z1} I_1^{-1} I_2}{\sum_i ((I_2^{-1} I_1 U_1 \vec{p}_1)^T I_2 I_1^{-1} F_{z1} I_1^{-1} I_2)_i} \\ &= \frac{(U_1\vec{p}_1)^T F_{z1} I_1^{-1} I_2}{\sum_i ((U_1\vec{p}_1)^T F_{z1} I_1^{-1} I_2)_i} \\ &= \vec{W}_1 I_1^{-1} I_2 \frac{\sum_i ((U_1\vec{p}_1)^T F_{z1})_i}{\sum_i ((U_1\vec{p}_1)^T F_{z1} I_1^{-1} I_2)_i}. \end{aligned} \quad \text{(D2)}$$

We see that if I_1 and I_2 only vary by a redshift-independent normalization factor, the effect on $\vec{W}$ cancels out entirely, and this is quite a good approximation at all redshifts of interest for the signal (see e.g. paper II [28]). Thus while the redshift dependence of $I_1^{-1} I_2$ *does* slightly distort the shape of the weighting function, the impact on the extracted f_{eff} is negligible (as demonstrated explicitly in Sec. III).

[1] J. A. Adams, S. Sarkar, and D. Sciama, Mon. Not. R. Astron. Soc. **301,** 210 (1998).

[2] X.-L. Chen and M. Kamionkowski, Phys. Rev. D **70,** 043502 (2004).

[3] N. Padmanabhan and D. P. Finkbeiner, Phys. Rev. D **72,** 023508 (2005).

[4] G. Hinshaw, D. Larson, E. Komatsu, D. N. Spergel, C. L. Bennett, J. Dunkley, M. R. Nolta, M. Halpern, R. S. Hill, N. Odegard et al., Astrophys. J. Suppl. Ser. **208,** 19 (2013).

[5] K. T. Story, C. L. Reichardt, Z. Hou, R. Keisler, K. A. Aird, B. A. Benson, L. E. Bleem, J. E. Carlstrom, C. L. Chang, H.-M. Cho et al., Astrophys. J. **779,** 86 (2013).

[6] Z. Hou, C. L. Reichardt, K. T. Story, B. Follin, R. Keisler, K. A. Aird, B. A. Benson, L. E. Bleem, J. E. Carlstrom, C. L. Chang et al., Astrophys. J. **782,** 74 (2014).

[7] J. L. Sievers et al. (Atacama Cosmology Telescope), J. Cosmol. Astropart. Phys. 10 (2013) 060.

[8] P. Ade et al. (Planck Collaboration), arXiv:1502.01589.

[9] L. Zhang, X. Chen, M. Kamionkowski, Z.-g. Si, and Z. Zheng, Phys. Rev. D **76,** 061301 (2007).

[10] G. Huetsi, A. Hektor, and M. Raidal, Astron. Astrophys. **505,** 999 (2009).

[11] M. Cirelli, F. Iocco, and P. Panci, J. Cosmol. Astropart. Phys. 10 (2009) 009.

[12] S. Galli, F. Iocco, G. Bertone, and A. Melchiorri, Phys. Rev. D **80,** 023505 (2009).

[13] T. R. Slatyer, N. Padmanabhan, and D. P. Finkbeiner, Phys. Rev. D **80,** 043526 (2009).

[14] T. Kanzaki, M. Kawasaki, and K. Nakayama, Prog. Theor. Phys. **123,** 853 (2010).

[15] J. Hisano, M. Kawasaki, K. Kohri, T. Moroi, K. Nakayama, and T. Sekiguchi, Phys. Rev. D **83,** 123511 (2011).

[16] G. Hutsi, J. Chluba, A. Hektor, and M. Raidal, Astron. Astrophys. **535,** A26 (2011).

[17] S. Galli, F. Iocco, G. Bertone, and A. Melchiorri, Phys. Rev. D **84,** 027302 (2011).

[18] D. P. Finkbeiner, S. Galli, T. Lin, and T. R. Slatyer, Phys. Rev. D **85,** 043522 (2012).

[19] T. R. Slatyer, Phys. Rev. D **87,** 123513 (2013).

[20] S. Galli, T. R. Slatyer, M. Valdes, and F. Iocco, Phys. Rev. D **88,** 063502 (2013).

[21] L. Lopez-Honorez, O. Mena, S. Palomares-Ruiz, and A. C. Vincent, J. Cosmol. Astropart. Phys. 07 (2013) 046.

[22] M. S. Madhavacheril, N. Sehgal, and T. R. Slatyer, Phys. Rev. D **89,** 103508 (2014).

[23] M. Valdes and A. Ferrara, Mon. Not. R. Astron. Soc. **387,** L8 (2008).

[24] M. Valdes, C. Evoli, and A. Ferrara, Mon. Not. R. Astron. Soc. **404,** 1569 (2010).

[25] S. R. Furlanetto and S. J. Stoever, Mon. Not. R. Astron. Soc. **404,** 1869 (2010).

[26] C. Evoli, M. Valdes, A. Ferrara, and N. Yoshida, Mon. Not. R. Astron. Soc. **422,** 420 (2012).

[27] J. M. Shull and M. E. van Steenberg, Astrophys. J. **298,** 268 (1985).

[28] T. R. Slatyer, Phys. Rev. D **93,** 023521 (2016).

[29] M. Cirelli, G. Corcella, A. Hektor, G. Hütsi, M. Kadastik, P. Panci, M. Raidal, F. Sala, and A. Strumia, J. Cosmol. Astropart. Phys. 03 (2011) 051.

[30] http://nebel.rc.fas.harvard.edu/epsilon.

[31] J. Zavala, M. Vogelsberger, and S. D. M. White, Phys. Rev. D **81,** 083502 (2010).

[32] S. Hannestad and T. Tram, J. Cosmol. Astropart. Phys. 01 (2011) 016.

[33] J. Chluba and R. A. Sunyaev, Mon. Not. R. Astron. Soc. **419,** 1294 (2012).

[34] J. Chluba, Mon. Not. R. Astron. Soc. **436,** 2232 (2013).

[35] G. Giesen, J. Lesgourgues, B. Audren, and Y. Ali-Haïmoud, J. Cosmol. Astropart. Phys. 12 (2012) 008.

[36] M. Farhang, J. R. Bond, and J. Chluba, Astrophys. J. **752,** 88 (2012).

[37] C. Weniger, P. D. Serpico, F. Iocco, and G. Bertone, Phys. Rev. D **87,** 123008 (2013).

[38] J. M. Cline and P. Scott, J. Cosmol. Astropart. Phys. 03 (2013) 044.

[39] P. Ciafaloni, D. Comelli, A. Riotto, F. Sala, A. Strumia, and A. Urbano, J. Cosmol. Astropart. Phys. 03 (2011) 019.

[40] http://www.marcocirelli.net/PPPC4DMID.html.

[41] M. Cirelli, M. Kadastik, M. Raidal, and A. Strumia, Nucl. Phys. **B813,** 1 (2009).

[42] M. Boudaud, S. Aupetit, S. Caroff, A. Putze, G. Belanger et al., Astron. Astrophys. **575,** A67 (2015).

[43] A. Lopez, C. Savage, D. Spolyar, and D. Q. Adams, arXiv:1501.01618.

[44] G. Steigman, B. Dasgupta, and J. F. Beacom, Phys. Rev. D **86,** 023506 (2012).

[45] M. Aartsen et al. (IceCube Collaboration), Phys. Rev. D **88,** 122001 (2013).

[46] M. Aartsen et al. (IceCube Collaboration), Eur. Phys. J. C **75,** 492 (2015).

[47] M. Aartsen et al. (IceCube Collaboration), Eur. Phys. J. C **75,** 20 (2015).

[48] R. T. D'Agnolo and J. T. Ruderman, Phys. Rev. Lett. **115,** 061301 (2015).

[49] E. Izaguirre, G. Krnjaic, P. Schuster, and N. Toro, Phys. Rev. Lett. **115,** 251301 (2015).

[50] O. Adriani et al. (PAMELA Collaboration), Nature (London) **458,** 607 (2009).

[51] M. Ackermann, M. Ajello, A. Allafort, W. B. Atwood, L. Baldini, G. Barbiellini, D. Bastieri, K. Bechtol, R. Bellazzini, B. Berenji et al., Phys. Rev. Lett. **108,** 011103 (2012).

[52] L. Accardo, M. Aguilar, D. Aisa, B. Alpat, A. Alvino, G. Ambrosi, K. Andeen, L. Arruda, N. Attig, P. Azzarello et al. (AMS Collaboration), Phys. Rev. Lett. **113,** 121101 (2014).

[53] I. Cholis and D. Hooper, Phys. Rev. D **88,** 023013 (2013).

[54] S. Seager, D. D. Sasselov, and D. Scott, Astrophys. J. Lett. **523,** L1 (1999).

[55] J. Chluba and R. M. Thomas, Mon. Not. R. Astron. Soc. **412,** 748 (2011).

[56] Y. Ali-Haimoud and C. M. Hirata, Phys. Rev. D **83,** 043513 (2011).

[57] A. Lewis, A. Challinor, and A. Lasenby, Astrophys. J. **538,** 473 (2000).